Transp. Infrastruct. Geotech. (2018) 5:169–186
https://doi.org/10.1007/s40515-018-0055-0

TECHNICAL PAPER

Effect of Load Eccentricity on the Bearing Capacity of Strip Footings on Non-homogenous Clay Overlying Bedrock

Mohamed Younes Ouahab[1] · **Abdelhak Mabrouki**[1] · **Mekki Mellas**[1] · **Djamel Benmeddour**[1]

Accepted: 3 April 2018 / Published online: 21 April 2018

Abstract In underwater infrastructure design, foundations are embedded in soft clay seabeds that exhibited non-homogeneity of cohesion, and subjected to combined actions of vertical, inclined or eccentric loads due to the environmental conditions such as self-weight, wind and wave forces acting on substructure. This paper investigates the undrained bearing capacity for surface and embedded strip footings on non-homogenous clay overlying bedrock. Elasto-plastic finite element analyses are carried out for perfectly rough strip footings on Tresca soil under vertical eccentric loads. Meyerhof's effective width rule is examined for the cases of surface and embedded footings in non-homogeneous clay. The effect of load eccentricity on the distribution of the normal stresses under strip footings is also investigated in this study. It is found that the effective width rule provides a conservative estimate of the bearing capacity. The elasto-plastic calculations predict that tensile stresses occur for surface footings because of the full bonding at the soil-footing interfaces, while for embedded footings, there is no tensile stresses.

✉ Mohamed Younes Ouahab
ouahabmy@gmail.com

Abdelhak Mabrouki
a.mabroukii@yahoo.fr

Mekki Mellas
m_mellas@yahoo.fr

Djamel Benmeddour
benmeddourdj@yahoo.fr

[1] Civil Engineering Research Laboratory LRGC, University of Biskra, BP 145, 07000 Biskra, Algeria

Keywords Bearing capacity · Non-homogeneous clay · Eccentric loading · Bedrock · Shallow footing

Introduction

Current studies of bearing capacity for shallow foundations assume that the soil layer below the footing extends to an infinite depth. In practice, the case of shallow footings on limited soil layer underlain by a rigid base, such as bedrock, located at a shallow depth below the footing can be encountered in the field of geotechnical engineering. The bearing capacity of shallow footings is traditionally estimated using the bearing capacity formula reported by [1]; this equation is valid for a situation where the shallow strip footing is subjected to centred vertical loads, which involves a symmetric failure mechanism. However, for complex models as load inclination, load eccentricity and footing embedment, Terzaghi's formula was modified through the addition of correction factors [2–4]. Also, the bearing capacity for strip footings under combined loading (vertical, inclined or eccentric loads) can be conveniently represented by failure envelopes.

The bearing capacity evaluation of shallow foundation using the failure envelope method is useful by comparing with the correction factor method. Representation of the bearing capacity as a failure envelope allows a direct evaluation of the margin of safety against failure with respect to changes in the individual load components.

In the literature, there are different methods to determine a failure envelope: experimental (e.g., [5–7]), theoretical and numerical analyses (e.g., [8–12]).

The effect of the presence of a rigid base on the bearing capacity of shallow footing on frictional soil has been addressed extensively through experimental studies ([13–17]). They found that the bearing capacity factor N_γ increases by the decrease in the soil layer thickness, and vice versa. However, very little work has addressed the bearing capacity of strip footing on a clay overlying bedrock.

For the case of strip footings on homogenous clay under pure vertical loads, Mandel and Salençon [18] have analysed the effect of the presence of a rigid base and its roughness on the bearing capacity using the limit equilibrium theory. They found that the bearing capacity depends on the footing width-to-thickness layer ratio B/h and on the interface contact between the soil layer and the rigid base. Matar and Salençon [19] obtained an exact solution for the bearing capacity of strip footings, under vertical loading, on a limited clay layer with a linear increase of cohesion with depth. The results were presented as a chart form.

In practice, footing never lies on the ground surface; it is mostly embedded in the soil at a depth D below the ground surface. Undrained bearing capacity of embedded footings has been investigated by several numerical studies ([20–25]). They found that the embedment depth has a significant effect on the bearing capacity.

Recently, the finite element method becomes a powerful tool to model complex geometries and soil parameters that affect the bearing capacity of shallow footings. The presence of a rigid base within the failure zone underneath footing in clayey soils is one of the special problems which are studied only for the case of strip footing under pure vertical loads. However, for the case of eccentrically loaded strip footings on non-homogeneous clay layer overlying bedrock, this problem is not yet studied.

In this paper, a series of numerical computations using the finite element code Plaxis [26] are carried out to evaluate the bearing capacity factors and the failure envelopes in a combined vertical-moment (*V-M*) loading plane. The problem studied considers surface and embedded strip footings under eccentric loads on a non-homogeneous clay layer overlying bedrock located at different depths below the strip footing. The rate κ of strength non-homogeneity, the soil layer thickness-to-footing width ratio h/B and footing embedment ratio D/B are investigated according to the load eccentricity e/B.

Presentation of the Problem

For the case of surface footing on non-homogeneous clay (Fig. 1), the undrained bearing capacity of strip footings is calculated as follows:

$$q_u = c_0 N'_c \tag{1}$$

where c_0 is the undrained shear strength at the ground surface (Fig. 1) and N'_c is the bearing capacity factor function of c_u. Hence, c_u is expressed as:

$$c_u = c_0 + k{\cdot}z \tag{2}$$

where c_u is the undrained shear strength, which varies linearly with depth, and k is the cohesion gradient with depth z.

For the case of embedded footing on non-homogeneous clay (Fig. 1), the undrained bearing capacity of strip footings is calculated as follows:

$$q_u = c_{u0} N^*_c \tag{3}$$

$$N^*_c = N'_c d_c \tag{4}$$

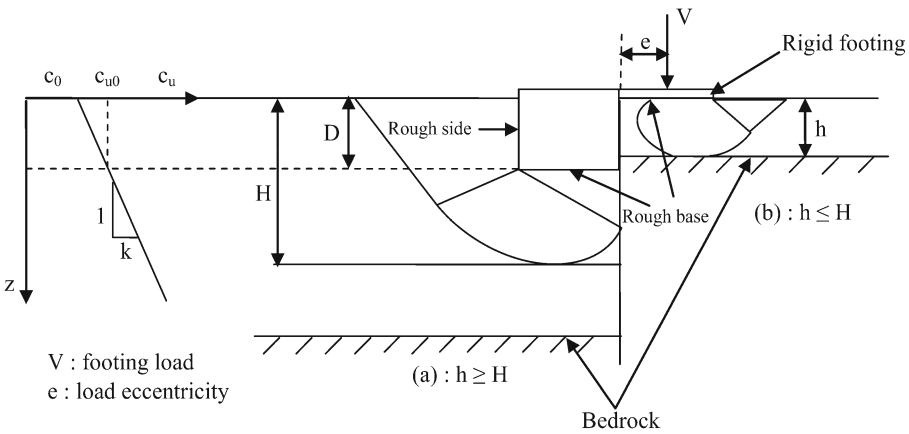

Fig. 1 Problem geometry. (a): Embedded footing and (b): surface footing

where N^*_c is the bearing capacity factor function of c_u and d_c is the depth factor. For the case of surface footing, d_c is equal to 1. The cohesion at the footing base level c_{u0} (Fig. 1) is expressed as:

$$c_{u0} = c_0 + kD \tag{5}$$

where D is the depth of the footing. The degree of non-homogeneity for a given foundation is represented by the non-dimensional ratio $\kappa = kB/c_0$, where B is the footing width.

The thickness of the non-homogeneous clay layer is represented by the non-dimensional soil layer thickness-to-footing width ratio h/B, while the embedment depth of the footing is represented by the non-dimensional ratio D/B.

The effective width approach reported by [2] assumes that the footing area is reduced corresponding to the effective width ($B' = B - 2e$) on which the loading is centrally applied. For embedded footing under eccentric loading, the bearing capacity q_u is expressed as:

$$q_c = N_{c0}\left(1-2\frac{e}{B}\right)c_u d_c \tag{6}$$

where N_{c0} is the theoretical bearing capacity factor for pure vertical loading, e is the load eccentricity, B is the footing width, c_u is the undrained shear strength of soil and d_c is the depth factor for footing on homogeneous clay which is expressed as $d_c = 1 + 0.2D/B$ [27], where D is the footing embedment.

Numerical Procedures

In this paper, the finite element code Plaxis [26] was used to evaluate the bearing capacity for surface and embedded strip footings on a non-homogeneous clay layer overlying bedrock. The strength non-homogeneity ratio κ ranges from 0 to 20 and the soil layer thickness h/B varies from 0.1 to 1 while the embedment depth D/B varies from 0 to 1.

Because of the absence of loading symmetry, the entire soil domain is modelled using 15-node elements. The right and left vertical sides of the models are constrained horizontally, while the bottom side was constrained in all directions.

A series of numerical computations are carried out to test the influence of the mesh size. In all cases, the mesh around the footing corners is refined. Potts and Zdravkovich [28] indicate that the mesh with smaller elements and a graded mesh under the corner of the footing produce more accurate solutions. The lateral boundaries of the adopted meshes for both finite and infinite soil layers were positioned $4.5B$ beyond the footing edges, while the bottom boundaries were positioned h/B and $5B$ below the ground surface respectively (Fig. 2).

In this study, the so-called probe loading technique is used. The footing load is applied in increments up to failure under load eccentricity e/B of 0.1, 0.2, 0.3 and 0.4, with respect to the reference point of pure vertical loading ($e/B = 0$). Each probe analysis leads to determine a single-failure load which is marked as a point in the failure envelope.

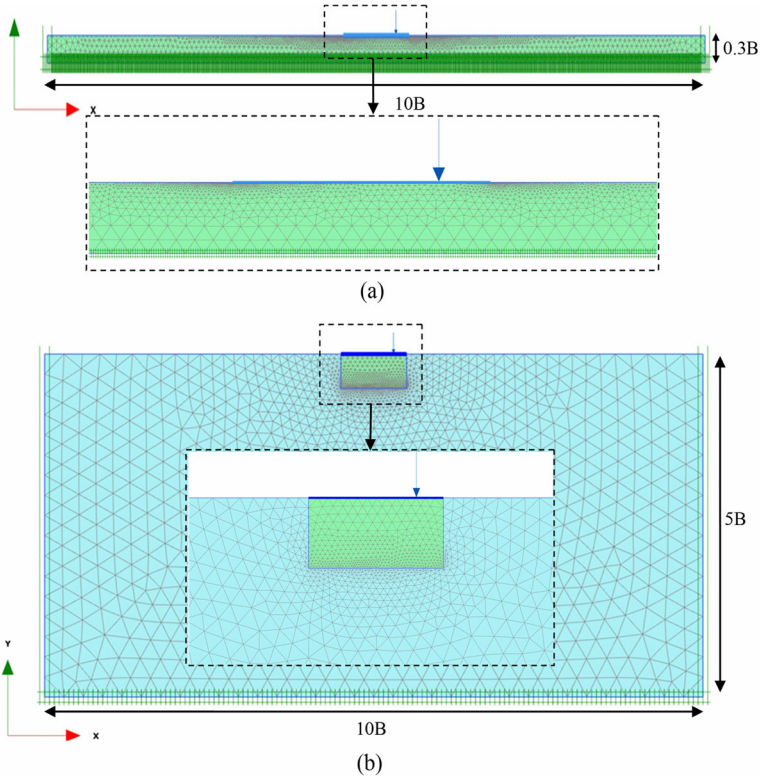

Fig. 2 Finite element mesh and boundary conditions. **a** Soil layer with $e/B = 0.3$ and $h/B = 0.3$. **b** Soil layer with $e/B = 0.3$ and $D/B = 0.5$

All finite element analyses were carried out for perfectly rough footings (no detachment at the soil-footing interface). The soil was modelled as a Tresca material ($\varphi = 0$, $\nu = 0.49$, $\gamma = 16$ kN/m^3). For undrained behaviour, Plaxis does not use a realistic bulk modulus of water, because this may lead to ill-conditioning of stiffness matrix and numerical problems. In fact, the total stiffness against isotropic compression of both soil and water is, by default, based on an implicit undrained bulk modulus $K_u = 2G(1 + \nu_u)/3(1 - 2\nu)$, where $\nu_u = 0.49$.

Young's modulus of soil was assumed to vary linearly with depth z ($E_u = E_0 + E_{inc} \cdot z$), where E_0 and E_{inc} are Young's modulus at the soil surface and the increment of Young's modulus per unit of depth respectively.

The surface footing was modelled as a non-porous linear elastic material with thickness $d = \sqrt{12EI/EA} = 1$ m, where $EI = 2.5$ GPa and $EA = 30$ GPa are the flexural rigidity (bending stiffness) and the axial stiffness respectively, while the embedded footing was modelled as a rigid body.

It should be noted that the values of the elastic parameters of the soil had no effect on the bearing capacity [29]. For surface footings resting on level ground, the undrained bearing capacity is insensitive to the soil unit weight γ [30].

The boundary conditions and typical finite element mesh of eccentrically loaded strip footing on finite and infinite non-homogeneous clay layers are shown in Fig. 2a, b respectively.

Verification of Numerical Results

For the case of strip footings on homogeneous soil ($\kappa = 0$), the exact solution obtained by [31] gives a value of the bearing capacity factor of 5.14 ($N_c = 2 + \pi$), while the finite element analysis, from the present study, gives a value of the bearing capacity factor of 5.144, in which the error is very much smaller than 0.04%.

The exact solution for the bearing capacity of strip footings, under pure vertical loading, on a finite clay layer with a linear increase of cohesion with depth, was obtained by [19] as follows:

$$q_u = p + \mu_c c_0 \left(N'_c + \frac{1}{4}\frac{kB}{c_0} \right) \tag{7}$$

where p is the uniform surcharge pressure and μ_c and N'_c are coefficients that are presented under a chart form, function of κ and h/B, from which they are read directly or interpolated.

Figure 3 shows a comparison of the obtained results, from this study, with those of the exact solution (Eq. 7) obtained by [19], for different values of soil strength non-homogeneity and for ratios $h/B = 0.16$, 0.25 and 0.5. The bearing capacity increases with increasing soil strength heterogeneity and decreases by increasing soil layer thickness h/B. The q_u values obtained are in excellent agreement with those of the exact solution of Matar and Salençon [19].

Figure 4 compares the obtained N'_c values of a rough strip footing on homogeneous clay ($\kappa = 0$), with the lower and upper bound values obtained by [8] for the case of surface footing ($D/B = 0$) on an infinite soil layer. It is clear that the bearing capacity factor N'_c decreases with increasing load eccentricity. The percentage of decrease in N'_c is of 55% for $e/B = 0.3$ by comparing with the cases of $e/B = 0$. The obtained numerical results of N'_c are in good agreement with those obtained by the lower and upper values reported by [8], except for the case of $e/B = 0.3$, where the numerical obtained results are slightly higher than the upper bound value.

Results and Discussion

Failure Loads

The effect of load eccentricity on the failure loads is shown in Fig. 5. The load-displacement curves from elasto-plastic finite element analysis are shown in Fig. 5a, for the case of surface footing ($D/B = 0$) on a non-homogeneous clay layer with $h/B = 0.1$, for the bounding cases of strength non-homogeneity $\kappa = 0$ and $\kappa = 20$, while Fig. 5b illustrates the load-displacement curves for the case of embedded strip footing ($D/B = 1$) on a homogeneous clay layer ($\kappa = 0$, $h/B = 5$). The curves are presented in terms of normalised applied loads V_u and displacements δ (V_u/Bc_0 versus δ/B).

The increase in the applied load is accompanied by the increase in the pressure under the footing until the stabilisation at a maximum value. This stabilisation is indicated in Fig. 5 by a plateau that corresponds to the bearing capacity q_u. It is clear that the

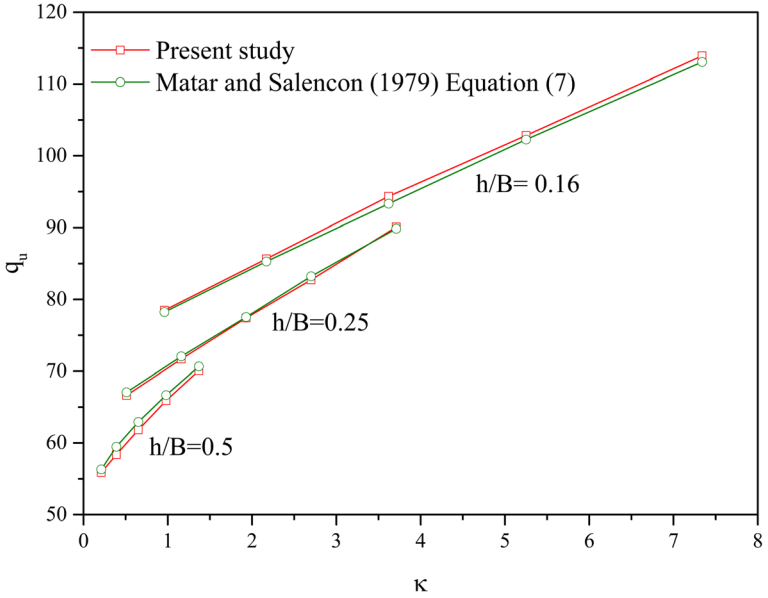

Fig. 3 Comparison of the obtained results with exact solution, for the case of undrained non-homogeneous clay

normalised failure loads decrease with increasing load eccentricity and increase with increasing strength non-homogeneity degree.

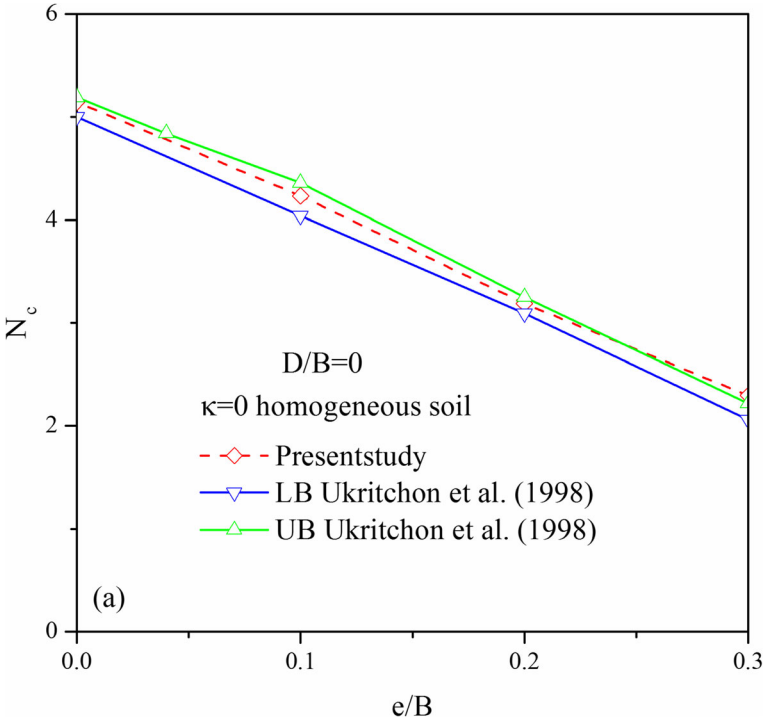

Fig. 4 Comparison of N'_c values, for the case of eccentric loading

Effect of the Presence of Bedrock

Figure 6a–d shows the effect of the presence of bedrock at shallow depths, below the surface strip footings, on the undrained bearing capacity. The results are presented in terms of bearing capacity factor $N_c^{'}$ with the variation in soil layer thickness ratio h/B, for different values of load eccentricity $e/B = 0$, 0.1, 0.2, 0.3 and 0.4, and soil strength heterogeneity $\kappa = 0$, 5, 10 and 20. It is seen that $N_c^{'}$ decreases with increasing soil layer thickness ratio until stabilises at a critical value of h/B in which the $N_c^{'}$ values become constant. When the soil layer thickness is greater than or equals the critical value, the effect of the presence of bedrock vanishes and the bearing capacity becomes constant.

For the case of homogeneous soil ($\kappa = 0$) and pure vertical loading ($e/B = 0$), Fig. 6a shows that $N_c^{'}$ decreases until stabilises at the classical value obtained by [31] ($N_c^{'} = \pi + 2$) corresponding to a critical value of $h/B \geq 0.7$, while for eccentric loading ($e/B > 0$), $N_c^{'}$ decreases until stabilises at a value less than the classical value of bearing capacity ($N_c^{'} < \pi + 2$). Besides, in the case of non-homogeneous soil ($\kappa > 0$), Fig. 6b–d shows that for all values of e/B, $N_c^{'}$ decreases with increasing soil layer thickness ratio until stabilises at a value corresponding to $h/B \geq 0.3$. The increase in $N_c^{'}$ with the decrease in h/B occurs for the reason that the presence of bedrock within the failure zone below the surface footing restricts the development of the failure mechanism and consequently leads to an increase in the bearing capacity.

The rate of the decrease in $N_c^{'}$ with increasing e/B is more significant in non-homogeneous clay ($\kappa > 0$) than in a homogeneous one ($\kappa = 0$). However, the decrease in $N_c^{'}$ with increasing h/B is more significant in homogeneous clay ($\kappa = 0$) than in a non-homogenous one ($\kappa > 0$), especially for high degrees of soil strength heterogeneity ($\kappa = 20$) where the bearing capacity is slightly affected. This occurs because the cohesion of soil increases with depth. Figure 7 shows that for all values of h/B, the bearing capacity factor $N_c^{'}$ decreases with increasing load eccentricity e/B and increases with increasing κ.

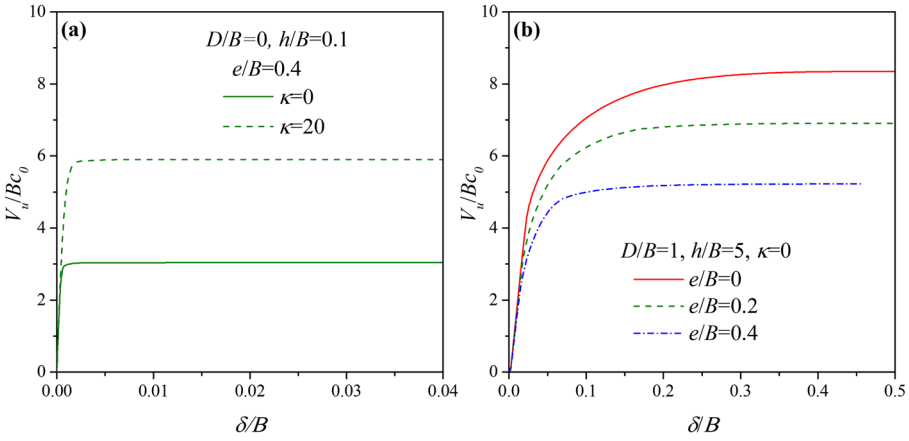

Fig. 5 Load-displacement curves. **a** Surface footing. **b** Embedded footing

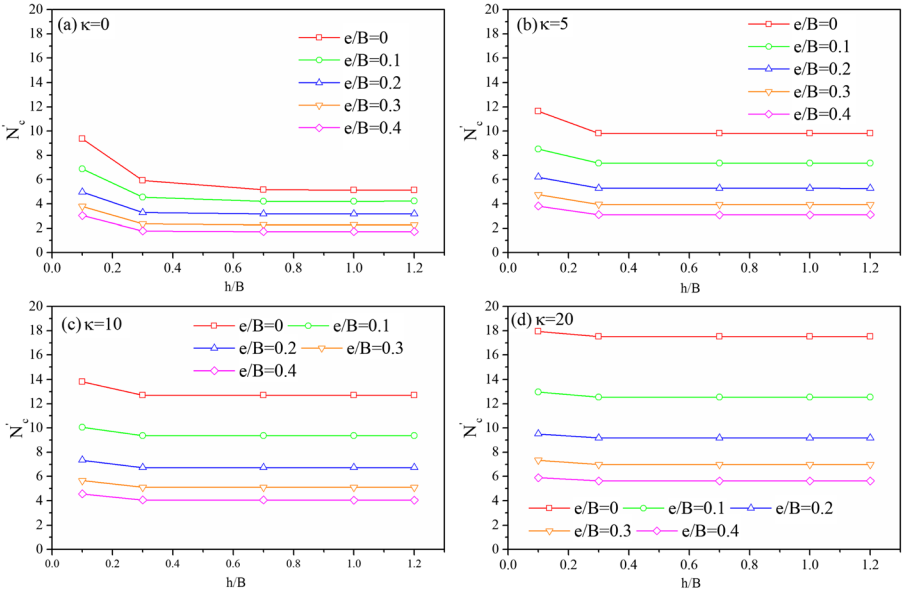

Fig. 6 Effect of h/B on N'_c

Effect of Footing Embedment

For the case of embedded footing in an infinite non-homogeneous clay layer, Fig. 8 shows the effect of embedment ratio D/B on the variation of N^*_c with e/B, for the bounding cases of soil strength heterogeneity $\kappa = 0$ and 20.

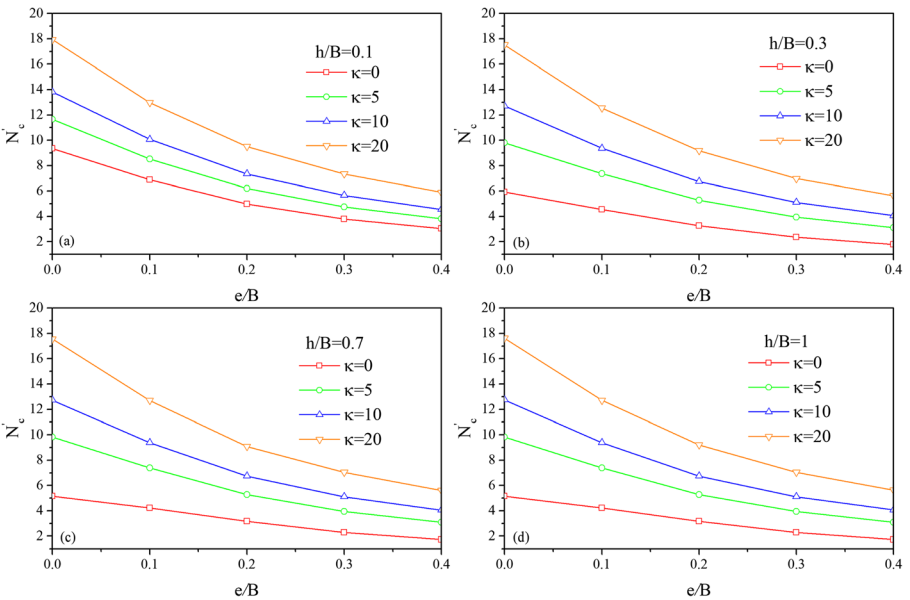

Fig. 7 Effect of κ and e/B on N'_c

For the case of homogeneous soil ($\kappa = 0$), Fig. 8a indicates that N^*_c increases with increasing footing embedment, while for the case of non-homogeneous soil ($\kappa = 20$), Fig. 8b indicates that, for all values of e/B, there is a predominant decrease in N^*_c for $D/B \leq 0.25$. A slight increase in N^*_c is remarked for the case of $e/B > 0$ and $D/B \geq 0.5$. Subsequently, it was found that there is no regular trend for the variation of the bearing capacity factor N^*_c, in which it depends on both c_{u0} and D/B. The variation of N^*_c with D/B is an effect of normalisation by the cohesion c_{u0} at the footing base level, while the bearing capacity q_u increases with D/B. For all values of D/B, the bearing capacity decreases with increasing load eccentricity. It can be seen that the rate of decrease in N^*_c with an increase in e/B is higher for non-homogeneous soil than that for a homogeneous one.

The variation of N^*_c function of e/B and κ is illustrated in Fig. 9, for the bounding cases of $D/B = 0$ and 1. For the case of surface footing ($D/B = 0$), Fig. 9a indicate that N^*_c increases by increasing soil strength non-homogeneity κ, while for the case of embedded footing ($D/B = 1$), Fig. 9b indicates that there is no significant effect of strength non-homogeneity ($\kappa = 5$, 10 and 20) on N^*_c. Also, Fig. 9b shows that, for low values of load eccentricity ($e/B \leq 0.16$), the N^*_c values are higher than those of N^*_c values when $e/B \geq 0.16$. An opposite tendency is observed between the homogeneous and non-homogeneous soils in which an intersection point at $e/B = 0.16$ is predicted according to an eccentricity $e = B/6$.

Assessment of Meyerhof's Effective Width Rule

A series of numerical computations using the effective width rule suggested by [2] are carried out through Plaxis. Figure 10 shows the vertical collapse loads V, determined from the results of eccentrically loaded footing ($e/B > 0$), normalised by the ultimate value V_{cent}, from the results of symmetrically loaded footing ($e/B = 0$), plotted against e/B, for surface and embedded strip footing with $\kappa = 0$ and 20. The obtained numerical results from analyses using full width footings (solid lines) are compared with those obtained from analyses using effective width footings (dash-dotted lines). The dotted lines representing the values from Meyerhof's solution (Eq. 6) are also shown. The values of the ratio V/V_{cent} decrease with an increase in load eccentricity e/B. It is

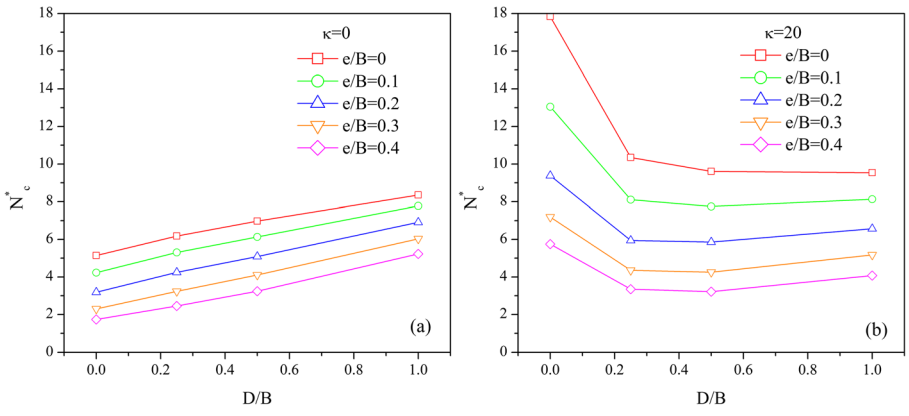

Fig. 8 Effect of D/B on N^*_c with e/B

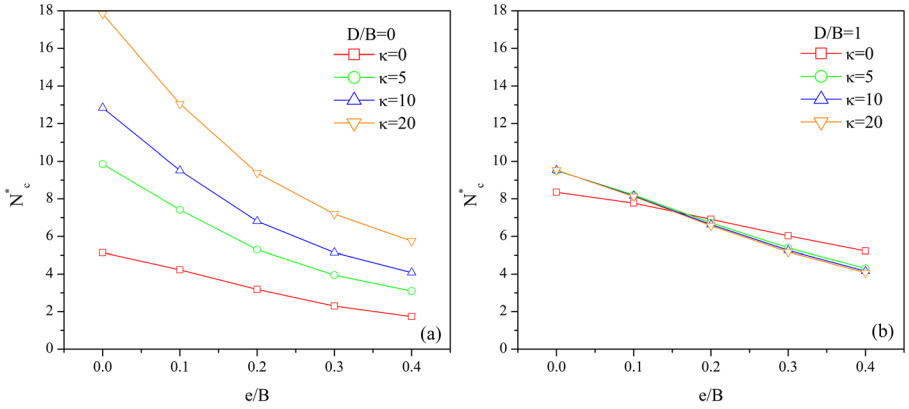

Fig. 9 Effect of e/B on N^*_c with κ

observed that, for both homogeneous and non-homogeneous soils, the effective width rule gives conservative values.

For a surface strip footing, the obtained numerical values are in good agreement with those of the effective width rule for $e/B < 0.2$ and $e/B < 0.1$ for homogeneous and non-homogeneous soils respectively. However, for the case of embedded footing, the obtained numerical values are larger than those of the effective width rule for all values of $e/B > 0$. It is worthwhile noting that the ratios V/V_{cent} obtained by the present study for embedded footings are substantially larger than those obtained when the footings located at the surface. Consequently, the footing embedment reduces the effect of load eccentricity. This occurs because of the effect of shear strength along vertical sides of embedded footing. An excellent agreement is obtained between the results of the present elasto-plastic analysis of surface and embedded footings by using effective

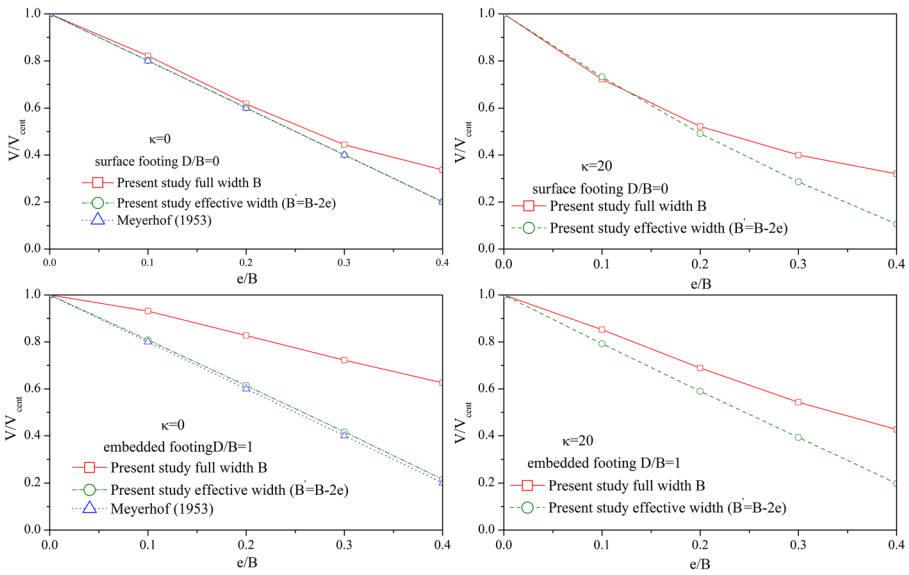

Fig. 10 Assessment of Meyerhof's effective width rule, for surface and embedded footing in non-homogeneous clay layers

width and the results of [2]. Application of the effective width rule gives a linear relationship between the ratio V/V_{cent} and load eccentricity e/B for homogeneous soil ($\kappa = 0$). However, for non-homogeneous soil ($\kappa = 20$), this relationship becomes non-linear.

Distribution of Normal Stresses

Distributions of the normal stresses σ_n at failure acting on the rough base of the strip footing are plotted in Fig. 11, for different values of the rate κ of strength non-homogeneity. The curves are presented in terms of both normalised normal stresses and horizontal distances from footing centreline (σ_n / c_0 versus x/B).

For the case of homogeneous soil ($\kappa = 0$), the distribution of the normal stresses is not uniform. This occurs because the settlement is uniform in the case of the rigid footing. The normal stress is larger in the footing edges and slightly decreases towards the footing centreline.

For the case of non-homogeneous soil ($0 < \kappa < 10$), the distribution of the normal stresses is not uniform and changes in size and shape as strength non-homogeneity increases. The magnitudes of normal stresses increase towards the centreline of the footing, while there is no increase along the footing edges. Figure 11 shows that the normal stresses σ_n increase with increasing strength non-homogeneity as the failure load.

For the case of homogeneous soil ($\kappa = 0$), Fig. 12 represents a comparison of the distribution of the normal stresses, with respect to the footing width, between the surface and embedded strip footings, for different values of $e/B = 0$, 0.2 and 0.4. Figure 12a shows the distribution of the normal stresses in the case of non-eccentric loading ($e/B = 0$), for surface and embedded strip footings. The normal stress

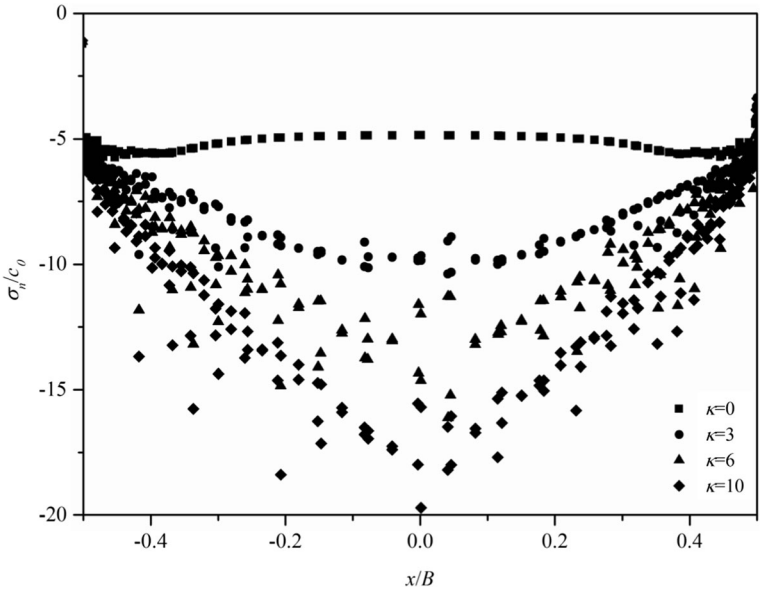

Fig. 11 Distributions of normal stress for the case of ($e/B = 0$)

distribution is symmetrical with respect to the centreline of the foundation in which the maximum values occurs at the right and left edges of the footing. Figure 12b, c shows that the distribution of normal stresses changes in terms of shape and size as the load eccentricity increases. The results show that for the case of surface footings ($D/B = 0$), tensile stresses occur at the left edge of the footing (< -0.5). This occurs because the full bonding at the soil-footing interfaces (no detachment), in which the loading is transmitted from the footing to the soil. For the case of embedded footings ($D/B = 1$), there is no tensile stresses. It is clear that the magnitude of the normal stresses, in the case of embedded footings, is greater than in the surface one.

Estimation of Bearing Capacity Using Advanced Method

The offshore foundations are subjected to combined loading (vertical load V, horizontal load H and moment M). The interaction of these load components must be explicitly taken into account when determining the load capacity. The advanced method consists to represent the ultimate limit states (bearing capacity) through interaction diagrams or failure envelope.

A failure envelope represents the yield locus in a vertical-moment loading plane. Every point in the failure envelope is obtained by a single-probe test analysis. The normalised failure envelopes (V/Bc_0-M/B^2c_0) for surface and embedded footings are shown in Figs. 13 and 14 respectively. It is clearly shown that the maximum moment capacity occurs at zero vertical loads. This happens because of the full adhesion along the footing-soil interface.

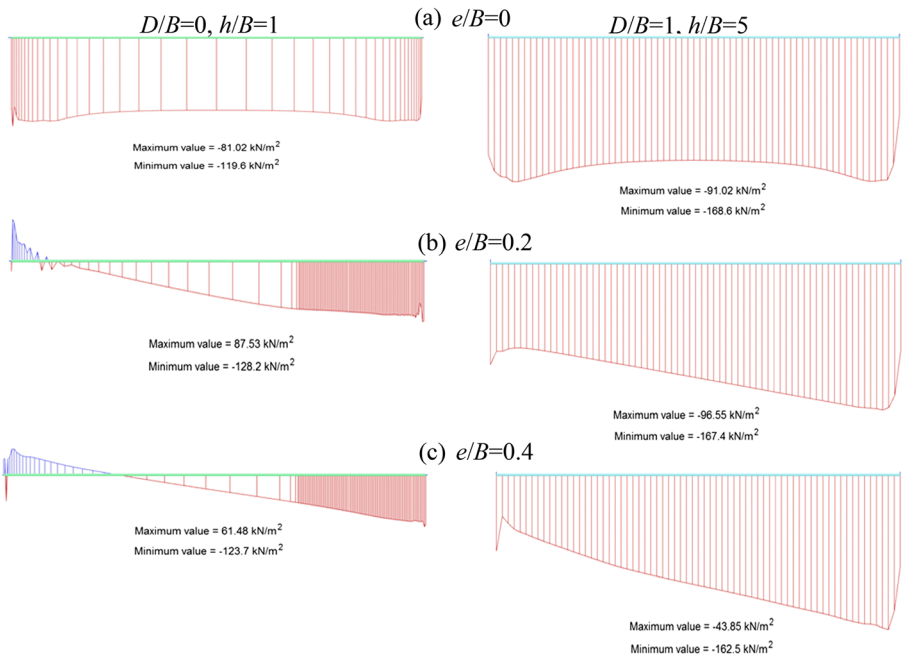

Fig. 12 Distributions of normal stress for the case of eccentric loading

Figure 13a–d illustrates the variation of the failure envelopes with h/B and κ. It can be seen that the sizes of the yield locus decrease by increasing soil layer thickness h/B. For the case of homogenous soil ($\kappa = 0$), the size of yield locus decreases by increasing h/B until stabilises at $h/B = 0.7$, while for the case of non-homogeneous soil ($\kappa > 0$), the size of the yield locus decreases by increasing h/B till stabilises at $h/B = 0.3$. It is seen that the size of the failure envelopes increases by increasing strength non-homogeneity ratio, from $\kappa = 0$ up to 20. For strip footing on a finite layer of $h/B = 0.1$, M/B^2c_0 is equal to 1.37 and 2.64 respectively for $\kappa = 0$ and 20. However, V/Bc_0 is equal to 9.36 and 17.94 respectively for $\kappa = 0$ and 20.

Figure 14a–d illustrates the variation of the failure envelopes with D/B and κ. For the case of homogeneous soil ($\kappa = 0$), the size of the yield locus increases with increasing footing embedment depth. However, for the case of non-homogeneous soil ($\kappa > 0$), the sizes of the yield locus are more diverse and show no regular trend for the distribution according to the embedment depth and soil strength non-homogeneity. The moment capacity of embedded strip footing ($D/B = 1$) in non-homogeneous soil is lower than that in a homogeneous one. The non-dimensional ratio M/B^2c_0 is equal to 2.38 and 1.64 respectively for $\kappa = 0$ and 20. Conversely, for vertical capacity, the non-dimensional ratio V/Bc_0 is equal to 8.35 and 9.53 respectively for $\kappa = 0$ and 20. This variation is attributed to the difference in the fail modes, between surface and embedded footings, according to the cohesion c_{u0} at the footing base level.

Failure Mechanisms

Contours of the incremental displacements, at failure, for rough strip footing are shown in the Fig. 15, for $\kappa = 0$ and $h/B = 0.3$. For purely vertical footing load ($e/B = 0$), the failure mechanism contains an elastic wedge zone located immediately below the

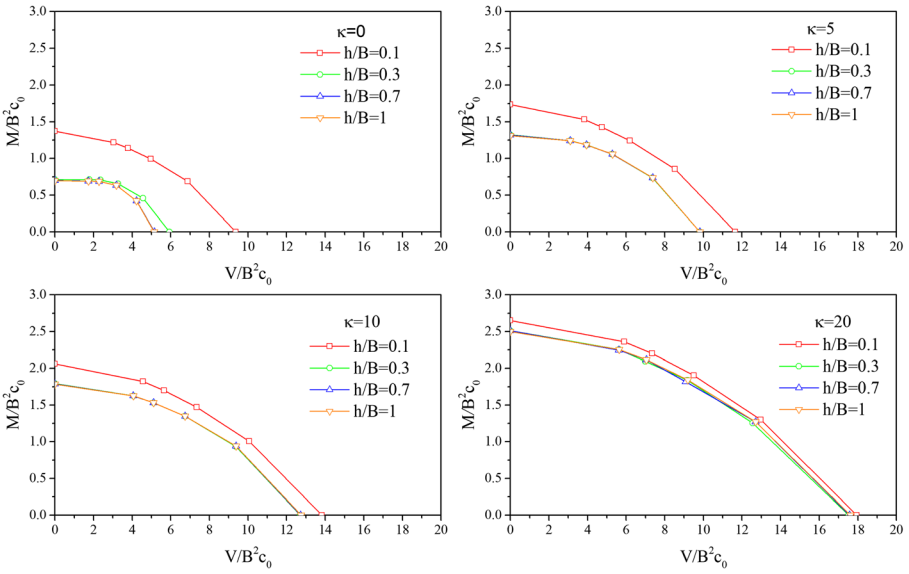

Fig. 13 Normalised failure envelopes and effect of h/B and κ

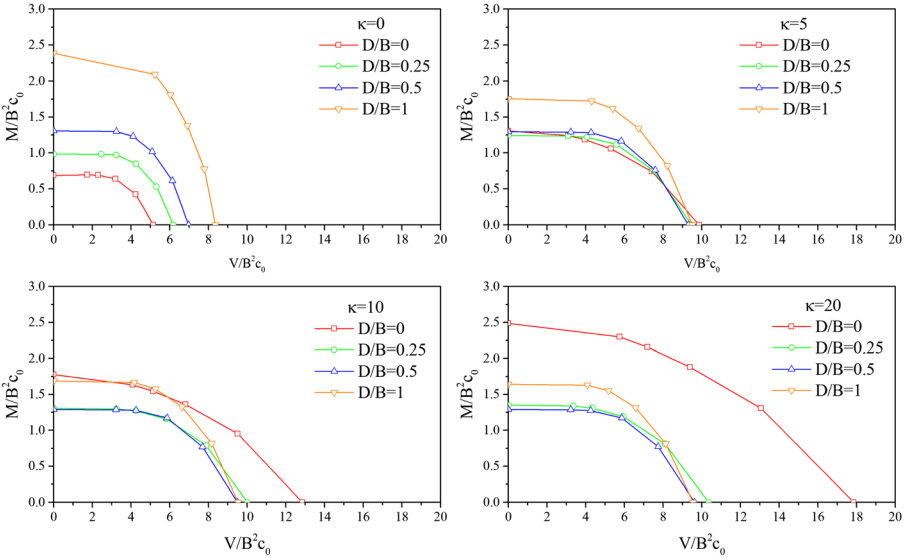

Fig. 14 Normalised failure envelopes and effect of D/B and κ

footing pushes away the soil in two symmetrical zones. The failure mechanism is symmetrical and similar to Terzaghi's one. Moreover, for eccentric footing loading ($e/B = 0.1, 0.2, 0.3$), the failure mechanisms contain a wedge and a scoop zones due to the vertical and moment loading effects respectively. It can be seen that the failure zones narrower as the load eccentricity increase. For the case of $e/B = 0.4$, the failure mechanism contains nearly a scoop zone.

The effect of the presence of bedrock on the development of the failure mechanisms is illustrated in Fig. 16. For the case of soil layer thickness of $h/B = 0.1$ and 0.3, the development of the failure mechanism is restricted which leads to an increase in the bearing capacity, while for $h/B = 0.7$, the failure mechanism is fully developed where the presence of bedrock does not affect the bearing capacity.

Conclusions

The finite element code Plaxis was used to investigate the undrained bearing capacity of eccentrically loaded strip footings on both finite and infinite non-homogenous clay layers. The aim of the work reported in this paper is the evaluation of new undrained bearing capacity factors and failure envelopes in a vertical-moment loading (V-M) plane. Meyerhof's effective width rule has been examined for the cases of surface and embedded footings in non-homogeneous clay. The effect of load eccentricity on the distribution of the normal stresses under the strip footings is also investigated in this study. A practical range of the rate κ of strength non-homogeneity, the soil layer thickness ratio h/B and the embedment ratio D/B was investigated. The results were compared with the available results published in the literature. Bearing capacity envelopes allowing direct evaluation of the margin of safety against failures are proposed in this study.

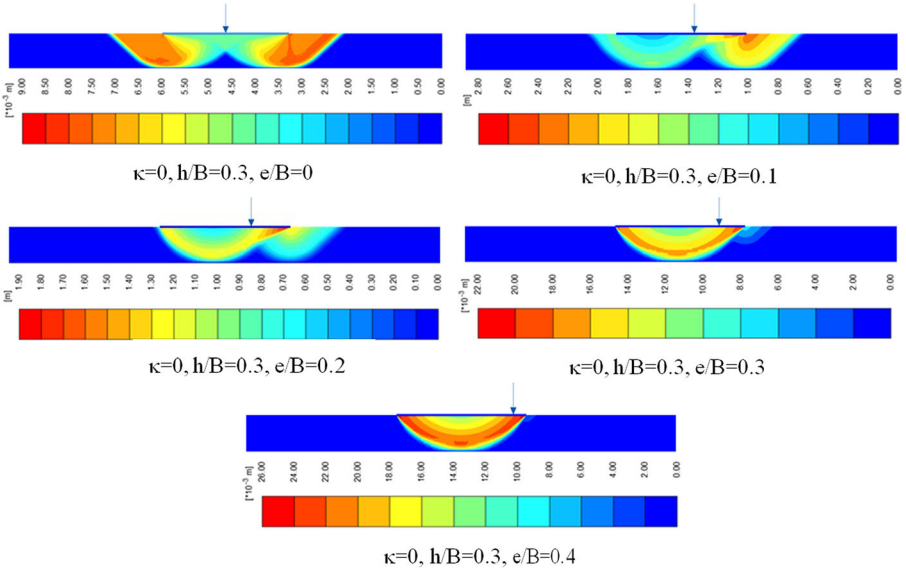

Fig. 15 Failure mechanisms, effect of e/B, and case of $\kappa = 0$ and $h/B = 0.3$

A new application of Meyerhof's effective width rule through elasto-plastic analyses for embedded footings in non-homogeneous soil leads to an excellent agreement with Meyerhof's solution. For both homogeneous and non-homogeneous soils, the effective width rule gives conservative values of the bearing capacity.

The bearing capacity factor $N_c^{'}$ for a surface strip footing on a finite clay layer increases with increasing soil strength heterogeneity and decreases with increasing h/B ratio until stabilises at critical values of 0.7 and 0.3 for homogeneous and non-

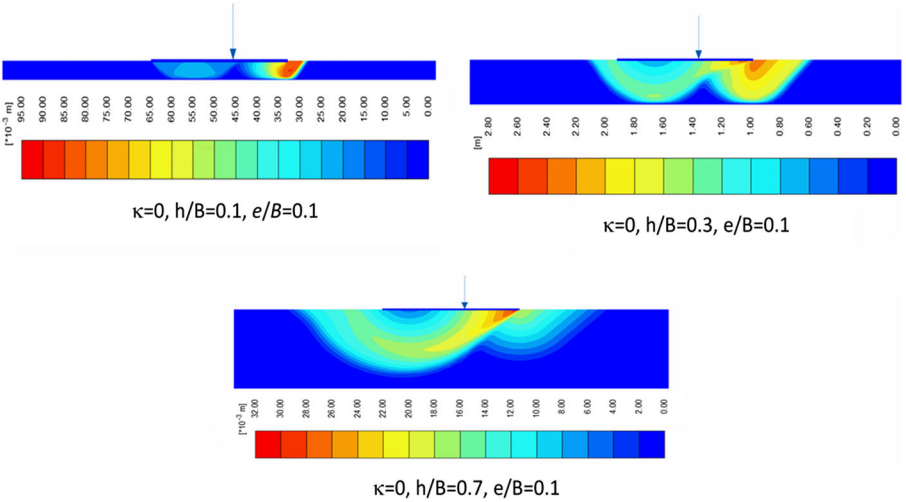

Fig. 16 Failure mechanisms, effect of h/B, and case of $\kappa = 0$ and $e/B = 0.1$

homogeneous soils respectively. The decrease in N'_c is more significant in the homogeneous clay than in the non-homogeneous one. The size of the yield locus is dependent on both strength non-homogeneity and soil layer thickness.

For embedded strip footings on the infinite clay layer, there is no regular trend in the variation of the bearing capacity factor N^*_c and the size of the failure envelopes. This variation is related to the value of the cohesion c_{u0} at the footing base level. The increase in the load eccentricity reduces both of N'_c and N^*_c.

For the case of homogeneous soil, the magnitude of normal stresses σ_n is larger in the footing edges and it decreases towards the footing centreline, while for the case of non-homogeneous soil, the magnitudes of normal stresses σ_n increase with the increasing strength non-homogeneity, where the maximum of these magnitudes occurs at the footing centreline. Tensile stresses are predicted for the case of surface footings because of the absence of detachment at the soil-footing interface, while there are no tensile stresses for the case of embedded footings.

The extent of the plastic zone below the strip footings is affected by the strength heterogeneity and the presence of bedrock at $h/B \leq 0.7$ and 0.3 for $\kappa = 0$ and $\kappa > 0$ respectively.

References

1. Terzaghi, K.: Theoretical Soil Mechanics. Wiley, New York (1943)
2. Meyerhof, G.T.: The bearing capacity of foundations under eccentric and inclined loads. In: *Proceedings, 3rd International Conference on Soil Mechanics and Foundation Engineering*, Zurich, **1**, 440–445 (1953)
3. Hansen, J.B.: A revised and extended formula for bearing capacity. Danish Geotech. Inst. Bull. **28**, 5–11 (1970)
4. Vesić, A.S.: Bearing capacity of shallow foundations. In *Foundation engineering handbook* (eds H. F. Winterkorn and H. Y. Fang). pp. 121-147. Van Nostrand Reinhold, New York (1975)
5. Nova, R., Montrasio, L.: Settlements of shallow foundations on sand. Géotechnique. **41**(2), 243–256 (1991)
6. Martin, C.M.: Physical and numerical modelling of offshore foundations under combined loads. DPhil thesis, University of Oxford (1994)
7. Gottardi, G., Houlsby, G., Butterfield, R.: Plastic response of circular footings on sand under general planar loading. Geotechnique. **49**(4), 453–469 (1999)
8. Ukritchon, B., Whittle, A.J., Sloan, S.W.: Undrained limit analyses for combined loading of strip footings on clay. J. Geotech. Geoenviron ASCE. **124**(3), 265–276 (1998)
9. Randolph, M.F., Puzrin, A.M.: Upper bound limit analysis of circular foundations on clay under general loading. Géotechnique. **53**(9), 785–796 (2003)
10. Gourvenec, S., Randolph, M.: Effect of strength non-homogeneity on the shape of failure envelopes for combined loading of strip and circular foundations on clay. Géotechnique. **53**(6), 575–586 (2003)
11. Loukidis, D., Chakraborty, T., Salgado, R.: Bearing capacity of strip footings on purely frictional soil under eccentric and inclined loads. Can. Geotech. J. **45**(6), 768–787 (2008)
12. Taiebat, H., Carter, J.: A failure surface for circular footings on cohesive soils. Geotechnique. **60**(4), 265–273 (2010)
13. Milovic, D.M., Tournier, J.P.: Comportement de fondations reposant sur une couche compressible d'epaisseur limitée. In: Proceedings of Conference Le comportement des sols avant la rupture, pp. 303–307. Paris, France (1971)
14. Pfeifle, T.W., Das, B.M.: Bearing capacity of surface footings on sand layer resting on a rigid rough base. Soils Found. **19**(1), 1–11 (1979)
15. Brown, R., Valsangkar, A.J., Schriver, A.B.: Centrifuge modeling of surface footings on a sand layer underlain by a rigid base. Geotech. Geol. Eng. **22**(2), 187–198 (2004)
16. Cerato, A.B., Lutenegger, A.J.: Bearing capacity of square and circular footings on a finite layer of granular soil underlain by a rigid base. J. Geotech. Geoenviron. **132**(11), 1496–1501 (2006)

17. Jun, S.H., Yoo, N.J., Yoo, K.S.: Bearing capacity of shallow foundation on a finite layer of sandy ground underlain by a rigid base. J. Kor. Geotech. Soc. **27**(6), 39–48 (2011)
18. Mandel, J., Salencon, J.: Force portante d'un sol sur une assise rigide (étude théorique). Géotechnique. **22**(1), 79–93 (1972)
19. Matar, M., Salençon, J.: Capacité portante des semelles filantes. Rev. Fr. Géotech. **9**, 51–76 (1979)
20. Salgado, R., Lyamin, A., Sloan, S., Yu, H.S: Two-and three-dimensional bearing capacity of foundations in clay. Géotechnique. **54**(5), 297–306 (2004)
21. Edwards, D.H., Zdravkovic, L., Potts, D.M.: Depth factors for undrained bearing capacity. Géotechnique. **55**(10), 755–758 (2005)
22. Gourvenec, S.M., Mana, D.S.K.: Undrained vertical bearing capacity factors for shallow foundations. Géotech. Lett. **1**(4), 101–108 (2011)
23. Bransby, M.F., Randolph, M.F.: The effect of embedment depth on the undrained response of skirted foundations to combined loading. Soils Found. **39**(4), 19–33 (1999)
24. Vulpe, C., Gourvenec, S., Power, M.: A generalised failure envelope for undrained capacity of circular shallow foundations under general loading. Géotech. Lett. **4**(3), 187–196 (2014)
25. Lee, J.K., Jeong, S., Lee, S.: Undrained bearing capacity factors for ring footings in heterogeneous soil. Comput. Geotech. **75**, 103–111 (2016)
26. Brinkgreve, R.B.J., Engin, E., Swolfs, W.M.: Plaxis user's manual. Plaxis, BV, Netherlands (2012)
27. Meyerhof, G.G: The ultimate bearing capacity of foundations. Géotechnique. **2**(4), 301–332 (1951)
28. Potts, D.M., Zdravković, L.: Finite element analysis in geotechnical engineering: Application. Thomas Telford, London (2001)
29. Mabrouki, A., Benmeddour, D., Frank, R., Mellas, M.: Numerical study of the bearing capacity for two interfering strip footings on sands. Comput. Geotech. **37**(4), 431–439 (2010)
30. Shiau, J.S., Merifield, R.S., Lyamin, A.V., Sloan, S.W.: Undrained stability of footings on slopes. Int. J. Geomechanics. **11**(5), 381–390 (2011)
31. Prandtl, L.: Über die härte plastischer körper. Nachr. Ges.Wiss. Goettingen Math. Phys. Kl., 74–85 (1920)